J Solid State Electrochem (2010) 14:889–895
DOI 10.1007/s10008-009-0875-5

ORIGINAL PAPER

Synthesis and electrochemical properties of nanosized carbon-coated $Li_{1-3x}La_xFePO_4$ composites

Dan Li · Yudai Huang · Dianzeng Jia · Zaiping Guo · Shu-Juan Bao

Received: 6 April 2009 / Revised: 24 May 2009 / Accepted: 26 May 2009 / Published online: 23 June 2009

Abstract Nanosized carbon-coated $Li_{1-3x}La_xFePO_4$ composites were synthesized using a fast, easy, microwave assisted, room-temperature, solid-state method. A lanthanum precursor was used to improve the electronic conductivity of $LiFePO_4$. The particle structure of the as-synthesized samples was observed using transmission electron microscopy. The results indicated that a uniform and continuous carbon layer was formed on the surface of $Li_{1-3x}La_xFePO_4$ particles. Electrochemical techniques, such as cyclic voltammetry, charge/discharge test, and electrochemical impedance spectroscopy were used to investigate the electrochemical performance of the samples. The results of electrochemical measurements revealed that the carbon coating and lanthanum doping provided an initial discharge capacity of 145 mA h/g with excellent rate capacity and long cycling stability. These advantages, coupled with the low cost, the high thermal stability, and the environmental friendliness of the raw materials, render $Li_{1-3x}La_xFePO_4$/C composites attractive for practical and large-scale applications.

Keywords $LiFePO_4$ · Lanthanum doping · Carbon coating · Lithium ion batteries · Cathode materials

D. Li · Y. Huang · D. Jia (✉) · S.-J. Bao
Institute of Applied Chemistry, Xinjiang University,
Urumqi 830046, China
e-mail: jdz@xju.edu.cn

Z. Guo
Institute for Superconducting and Electronic Materials,
University of Wollongong,
Wollongong 2522 NSW, Australia

Z. Guo
School of Mechanical, Materials and Mechatronic Engineering,
University of Wollongong,
Wollongong 2522 NSW, Australia

Introduction

Since the work of Padhi et al. [1], $LiFePO_4$ has become of great interest as a storage cathode material for rechargeable lithium ion batteries because of its high lithium intercalation voltage (~3.5 V relative to lithium metal), high theoretical capacity (170 mA h/g), environmental friendliness, low cost, and safety. This material is suitable for large-size applications, such as hybrid electric vehicles, electric vehicles, power tools, and electric bicycles [2]. Nevertheless, it is a mixed ionic-electronic conductor in which the lithium ion diffusion and the poor electronic conductivity dominate the transport phenomena [3]. To improve the conductivity of $LiFePO_4$, some approaches that have been used include coating particles with carbon [4] or co-synthesizing the compounds with carbon [5] to surround each particle with a good electronic conductor [6]. From a review of previous reports on carbon-coating techniques, the carbon layer is always incomplete and partially discontinuous [7, 8], which becomes problematic for omnidirectional lithium ion permeation. There have also been attempts to increase the inherent conductivity or chemical diffusion coefficient of lithium within the crystal by doping it with a supervalent ion [8–10]. Partial supervalent ion substitution could form suitable interstices for insertion and extraction of lithium ions in $LiFePO_4$. Compared with previous studies [8, 11–13], which always focused on only one aspect of improvement, the combined effects of carbon coating and cation doping on the electrochemical performance of materials could attract extensive interest.

A variety of material processing methods have been proposed to prepare $LiFePO_4$ for use as a cathode material, such as solid-state reaction [14, 15], sol-gel preparation [16, 17], hydrothermal reaction [18–20], and a co-precipitation

procedure [3, 21]. However, some reported methods require high-temperature annealing to achieve the carbonization and crystallization of the materials, which will lead to an increase in the particle size and affect the electrochemical performance of the materials correspondingly. In contrast, room-temperature solid-state reaction is believed to be an easy and effective way to fabricate a number of chemical compounds [22, 23], because it has the advantages of low energy consumption, convenient operation, and environmental benignity. To meet the requirements of developing economic and efficient synthesis routes, the use of microwave methodology allows faster reaction and avoids high-temperature synthesis [24].

In this work, a microwave assisted room-temperature solid-state method is proposed to prepare $Li_{1-3x}La_xFePO_4$ through the combination of surface coating and cation doping. The microstructure, morphology, and electrochemical performance of the as-synthesized products were investigated. The obtained nanosized $Li_{1-3x}La_xFePO_4/C$ composites exhibit a core-shell structure with a typical nanocrystalline $Li_{1-3x}La_xFePO_4$ core and a carbon shell, and show good rate capacity and long cycling stability.

Experimental

$Li_{1-3x}La_xFePO_4/C$ (x=0, 0.005, 0.01, 0.015, 0.02, 0.025) materials were prepared by room-temperature solid-state reaction and a microwave heating process. The preparation process is shown in Fig. 1. Stoichiometric $CH_3COOLi{\cdot}2H_2O$ and $(NH_4)_2HPO_4$ were ground in an agate mortar with a pestle for ~30 min to form a homogenous mixture, which was subject to a one-step solid-state reaction [25, 26]. These solid starting materials changed to a soft and pulpy mixture, and then changed into solid powders. Then, $FeC_2O_4{\cdot}2H_2O$, and a small quantity of citric acid without La_2O_3 were added and mixed for ~15 min. Later, a self-assembly carbon seal reactor with the precursors inside was put into a microwave oven (3.0 GHz, 850 W). After 15 min of microwave irradiation, a carbon shell, obtained by expansion of citric acid after being heated, formed a coating on the surfaces of the $Li_{1-3x}La_xFePO_4$ particles to yield the $Li_{1-3x}La_xFePO_4/C$ materials. A stereomicroscopic picture of the carbon decomposed from citric acid is embedded in Fig. 1. It is considered that the expansion of citric acid reduced the surface tension of the precursors and prevented the particles from growing in size [26].

The crystalline phase of the resulting materials was analyzed by powder X-ray diffraction (XRD, MXP18AHF, MAC, Japan), which was carried out using Cu Kα radiation (λ=1.54056 Å). The morphology of the decomposed carbon was characterized by stereomicroscopy (Leica, EZ4, Switzerland). The grain size and structure of the samples were observed using transmission electron microscopy (TEM, H-600, Hitachi, Japan) with an accelerating voltage of 100 kV and high-resolution transmission electron microscopy (HRTEM, JEOL JEM-2100, Japan) operating at 200 kV. Energy dispersive spectroscopy (EDS) was applied to examine the composition and distribution of elements in the materials. The surface morphology of the samples was observed by a scanning electron microscope (SEM, JEOL, JSM-6460A, Japan).

To prepare the working electrodes, the cathode slurry for testing was prepared by thoroughly mixing 85 wt.% active materials, 10 wt.% acetylene black, and 5 wt.% poly (vinylidene fluoride) in *N*-methylpyrrolidinone solvent. The obtained slurry was then spread onto an aluminum foil substrate and dried in a vacuum oven at 120°C for 12 h. The cells were composed of a lithium foil anode, the prepared active material as the cathode, microporous polyethylene (Celgard 2400) as the separator, and 1 M $LiPF_6$ in a mixture of ethylene carbonate and dimethyl

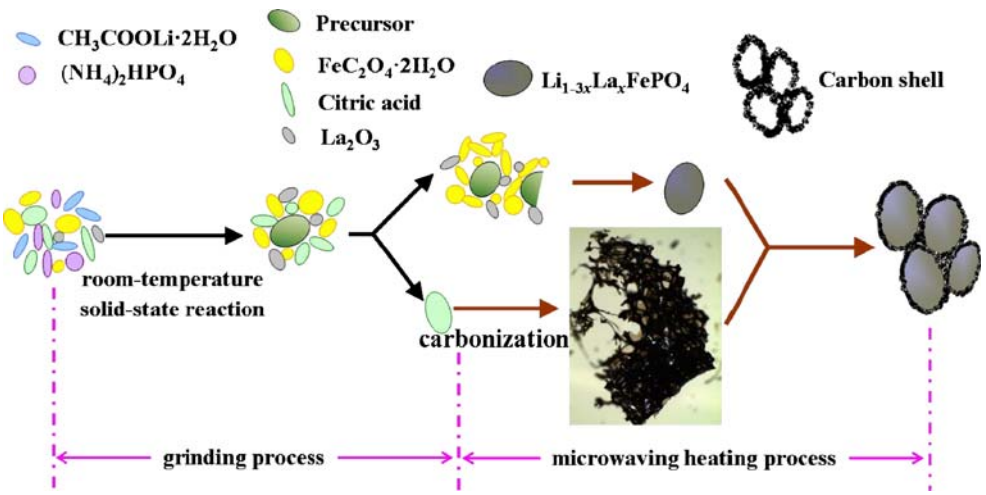

Fig. 1 Synthesis process for the $Li_{1-3x}La_xFePO_4/C$ samples

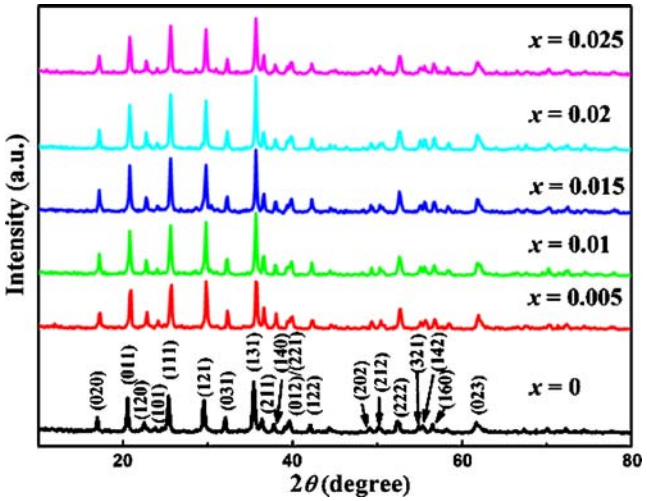

Fig. 2 XRD patterns of the $Li_{1-3x}La_xFePO_4/C$ (x=0, 0.005, 0.01, 0.015, 0.02, 0.025) samples

carbonate (1:1 by volume) as the electrolyte. The whole assembly process was carried out in an argon-filled glove box. The electronic conductivity of all the prepared samples was measured by the four-electrode method using a SDY-4 instrument (SDY-4, China). Cyclic voltammograms (CVs) were collected at a scan rate of 0.1 mV/s from 2.5 to 4.1 V, using a CHI660B electrochemical workstation (CHI, 660B, CHENHUA, China). Electrochemical impedance spectroscopy (EIS) was conducted over the 0.1 to 100 kHz frequency range using a Zahner Elektrik electrochemical workstation (IM6e, Zahner, Germany), which applied a dc potential equal to the open circuit voltage of the cell and an ac oscillation of 5 mV. The charge/discharge cycling was performed within a voltage range of 2.5–4.1 V on a battery test instrument (CT2001A, KINGNUO, China) at ambient temperature.

Results and discussion

Figure 2 shows the XRD patterns of the $Li_{1-3x}La_xFePO_4/C$ (x=0, 0.005, 0.01, 0.015, 0.02, 0.025) materials. All of the samples exhibit pure single phase $LiFePO_4$ with an ordered olivine structure indexed with the orthorhombic *Pnmb* space group (JCPDS card no. 40-1499). The lanthanum doping does not destroy the lattice structure of $LiFePO_4$ due to the low doping content of lanthanum. In spite of the carbon coating, no carbon peak can be observed from the XRD patterns due to the small amount and amorphous characteristics of the carbon. It is obvious that the diffraction peaks of the doped samples exhibit a rightward shift in 2θ compared with un-doped $LiFePO_4/C$, which indicates the influence of the lanthanum doping on the lattice parameters. The $Li_{1-3x}La_xFePO_4/C$ (x=0.02) sample, which exhibited better electrochemical performance, was chosen for study of the physical properties. The crystal parameters of the $Li_{1-3x}La_xFePO_4/C$ (x=0, 0.02) materials were calculated from the XRD patterns and are summarized in Table 1. As can be seen from these data, the crystal cell shows a slight contraction in both the a and b directions due to the strong binding force between lanthanum ions and oxygen ions. However, the c axis is slightly elongated because the ionic radius of the lanthanum ions (0.106 nm) is bigger than that of the lithium ions (0.076 nm) [27]. Furthermore, the b-axis direction is considered to be the most likely path for lithium ion migration [28], so the shortened lattice parameter b would make lithium ion motion easier.

In order to check the surface structure of the as-synthesized $Li_{1-3x}La_xFePO_4/C$ materials, TEM and HRTEM observations were carried out and are shown in Fig. 3. As shown in Fig. 3a and b, the particles are uniform in shape with the grain size ranging from 25 to 50 nm. Carbon has a significant effect on the formation of homogeneous nanosized $LiFePO_4$ particles because it plays a role in hindering particle growth during the heat treatment [2, 29]. In particular, microwave heating can tremendously decrease reaction time, and this will encourage the formation of nanosized particles. The $Li_{1-3x}La_xFePO_4/C$ (x=0.02) nanopowder with a particle size of about 25 nm is uniformly coated by an amorphous carbon layer, as can be observed in Fig. 3c. The carbon layer, which totally covers the primary $Li_{1-3x}La_xFePO_4$ crystallite to form a core-shell structure, is sufficient to create an electrically conducting layer. The interplanar spacing in the particle is 0.294 nm and matches well with the (121) plane of $LiFePO_4$. A fast Fourier transform analysis (inset in Fig. 3c) was performed on a selected region of the particle, which confirms that it is strictly oriented. Figure 3d shows two particles in an amorphous carbon matrix. This demonstrates that the carbon fully connects the $LiFePO_4$ particles through the expansion of citric acid after it is heated. The composition and distribution of elements in the $Li_{1-3x}La_xFePO_4/C$ (x= 0.02) sample were examined by EDS, as shown in Fig. 4. The bright spots correspond to the presence of the elements Fe, P, and La, respectively. The results show that Fe, P, and La are distributed uniformly throughout the whole area,

Table 1 Calculated crystal parameters of the $Li_{1-3x}La_xFePO_4/C$ (x=0, x=0.02) samples

$Li_{1-3x}La_xFePO_4/C$	a (Å)	b (Å)	c (Å)	Volume of unit cell (Å^3)
x=0	6.02289	10.50832	4.67915	296.15
x=0.02	5.99432	10.33436	4.69094	290.59

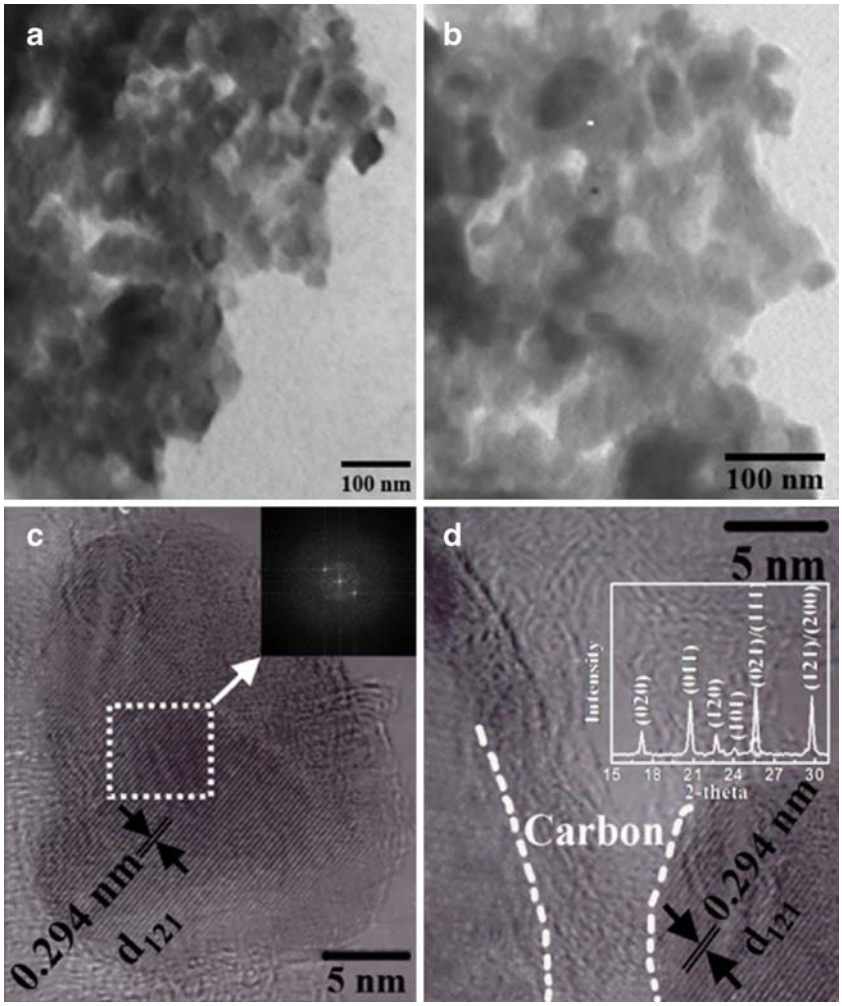

Fig. 3 TEM images of the $Li_{1-3x}La_xFePO_4/C$ samples: **a** $x=0$ and **b** $x=0.02$; **c** and **d** HRTEM images of the $Li_{1-3x}La_xFePO_4/C$ ($x=0.02$) sample. The *inset* in (**c**) shows the fast Fourier transform pattern that corresponds to the indicated region. The *inset* in (**d**) shows the XRD pattern corresponding to the indicated lattice spacing

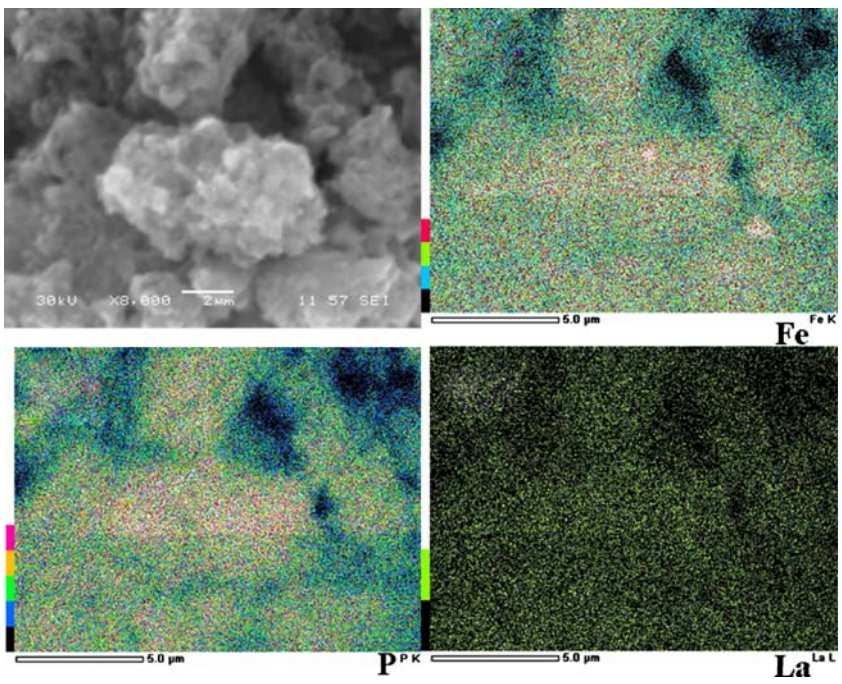

Fig. 4 Elemental mapping by SEM of the $Li_{1-3x}La_xFePO_4/C$ ($x=0.02$) sample

which indicates that La is distributed uniformly in the lanthanum-doped $LiFePO_4$ samples.

The electronic conductivity of the $Li_{1-3x}La_xFePO_4/C$ (x=0, 0.005, 0.01, 0.015, 0.02, 0.025) samples was measured by the four-electrode method, and the results are shown in Fig. 5. The conductivity of the as-synthesized $LiFePO_4/C$ sample increases by a factor of ~10^4 compared with that of pure $LiFePO_4$ ($\sigma \sim 10^{-9}$). It is believed that the network structure of carbon lowers contact resistance between the $LiFePO_4$ particles and makes the electronic conduction feasible [10]. It is also found that the conductivity is enhanced with increasing lanthanum doping. The $Li_{1-3x}La_xFePO_4/C$ (x=0.02) sample exhibits the highest electronic conductivity among all the samples, a factor of ~10^2 higher than that of un-doped $LiFePO_4/C$. However, further increasing the lanthanum doping level to x=0.025 induces a slightly decreased conductivity, 2.3×10^{-3} S/cm.

CVs were collected to investigate the changes in the electrochemical performance of the $Li_{1-3x}La_xFePO_4/C$ (x=0, 0.005, 0.01, 0.015, 0.02, 0.025) samples at the scanning rate of 0.1 mV/s over a voltage range of 2.5–4.1 V. Figure 6 compares different CV profiles of these cathodes in the first cycle. These similar CV curves with a pair of peaks (an anodic and a cathodic peak) reveal the single-electron reaction mechanism of $LiFePO_4$. The shape of the CV profiles becomes sharp with increasing dopant content. This could be ascribed to the decreased contact resistance because of the presence of the carbon network and the enhanced electronic conductivity of the lanthanum substituted samples. However, the CV profile of $Li_{1-3x}La_xFePO_4/C$ (x=0.025) possesses broadened peaks and a lower peak height. It is considered that excessively high dopant content could reduce the amount of lithium ions in the intercalation and deintercalation processes. The role of lanthanum doping can be further understood by comparing the CV curves of

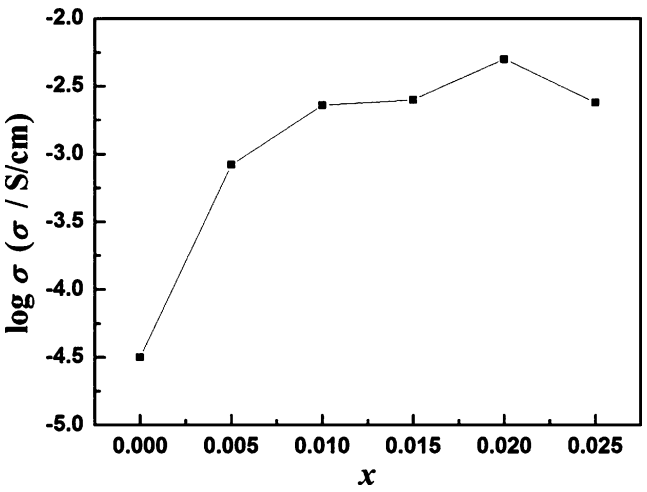

Fig. 5 Electronic conductivity of the $Li_{1-3x}La_xFePO_4/C$ (x=0, 0.005, 0.01, 0.015, 0.02, 0.025) samples at room temperature

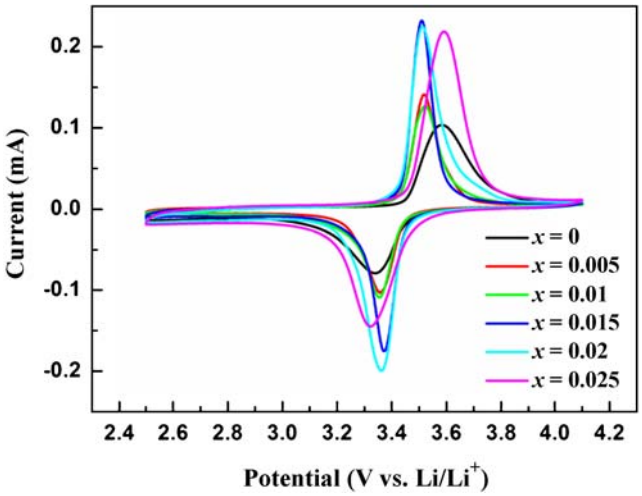

Fig. 6 CVs showing the first cycles for the $Li_{1-3x}La_xFePO_4/C$ (x=0, 0.005, 0.01, 0.015, 0.02, 0.025) samples

pure and doped samples, which show that the latter has better electrochemical performance. For $Li_{1-3x}La_xFePO_4/C$ (x=0.02), the voltage separation (0.147 V) is smaller than that of $LiFePO_4/C$ (0.241 V), and the narrower voltage separation and symmetric CV profile indicate that the sample has good reversibility.

Charge/discharge tests were carried out to clarify the cycling performance of these materials. Figure 7 presents the initial charge/discharge curves of these samples when the Li | $Li_{1-3x}La_xFePO_4/C$ (x=0, 0.005, 0.01, 0.015, 0.02, 0.025) cells were cycled at a current rate of 1.5 C from 2.5 to 4.1 V. The plateaus of the charge and discharge curves correspond to the reaction between $LiFePO_4$ and $FePO_4$. A stable flat voltage plateau appears in the discharge curves and then falls to the cut-off voltage value. For the $Li_{1-3x}La_xFePO_4/C$ (x=0.02) sample, the electrochemical

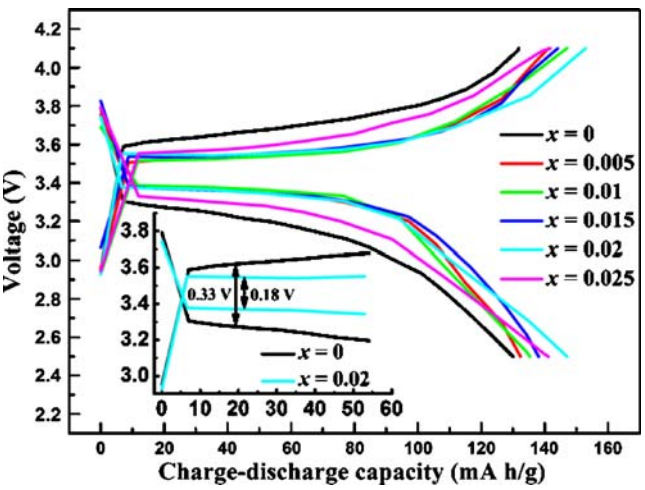

Fig. 7 The initial charge/discharge curves of the $Li_{1-3x}La_xFePO_4/C$ (x=0, 0.005, 0.01, 0.015, 0.02, 0.025) samples at a current rate of 1.5 C. The *inset* shows the initial flat region magnified

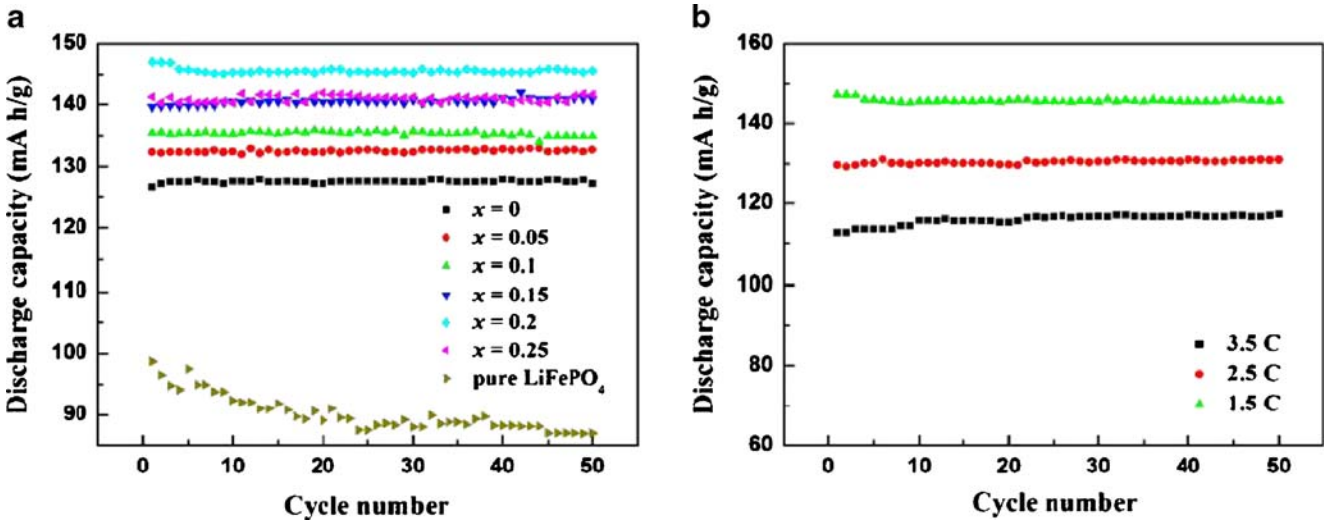

Fig. 8 Cycling performance of **a** the pure $LiFePO_4$ and the $Li_{1-3x}La_xFePO_4/C$ (x=0, 0.005, 0.01, 0.015, 0.02, 0.025) samples at 1.5 C and **b** the $Li_{1-3x}La_xFePO_4/C$ (x=0.02) sample at different current rates

polarization between the charge and discharge plateaus is reduced to 0.18 V compared with 0.33 V for the $LiFePO_4$/C sample, which proves that $Li_{1-3x}La_xFePO_4/C$ (x=0.02) possesses better kinetics [30]. The possible reason for this phenomenon is the synergetic effect of the enhanced electric conductivity by carbon coating and accelerated movement of lithium ions through lanthanum doping.

The cycling performance of the pure $LiFePO_4$ and the $Li_{1-3x}La_xFePO_4/C$ (x=0, 0.005, 0.01, 0.015, 0.02, 0.025) samples at 1.5 C is shown in Fig. 8a. The capacity of pure $LiFePO_4$ fades obviously with further cycling, and it drops from 97.9 mA h/g to 89 mA h/g after 50 cycles. However, the samples of carbon-coated $LiFePO_4$ demonstrate dramatically improved reversible capacity and cycling stability. With increasing doping level, progressive improvement of the discharge capacity is observed. When the amount of lanthanum goes up to x=0.02, the sample achieves the best cycling performance, with an average discharge capacity of 145 mA h/g. According to the doping mechanism proposed by Chung et al. [6], supervalent cations could partially substitute for lithium ions in the $LiFePO_4$ crystal lattice, which tends to enhance the intrinsic electronic conductivity and lithium ion diffusion in the doped samples. As a result, the discharge capacity is larger than that of the un-doped $LiFePO_4$/C sample. Figure 8b presents the rate performance of the $Li_{1-3x}La_xFePO_4/C$ (x=0.02) material measured at various rates. It is obvious that the sample demonstrates good cycling performance and rate capability, even at the higher rate of 3.5 C (average discharge capacity of 116 mA h/g). The doped samples exhibit larger capacity and better cycling performance at the high rate current than those $LiFePO_4$ samples reported in the literature that were doped with other elements [31–33]. The better cycling performance could be attributed to the small particle distribution, high phase purity, and improved conductivity through carbon-coating and lanthanum doping.

The kinetic processes of the $Li_{1-3x}La_xFePO_4/C$ (x=0, 0.005, 0.01, 0.015, 0.02, 0.025) samples are clearly depicted by EIS measurements. Figure 9 shows typical Nyquist plots of these samples, which are comprised of depressed semicircles and straight lines in different frequency regions. In the high-frequency region, the intercept with the real impedance axis corresponds to the ohmic resistance, which represents the total electric resistance of the electrode materials, the electrolyte resistance, and the resistance of the electric leads [34]. The numerical value of the diameter of the semicircle is approximately equal to the charge transfer resistance (R_{ct}). The inclined line in the low

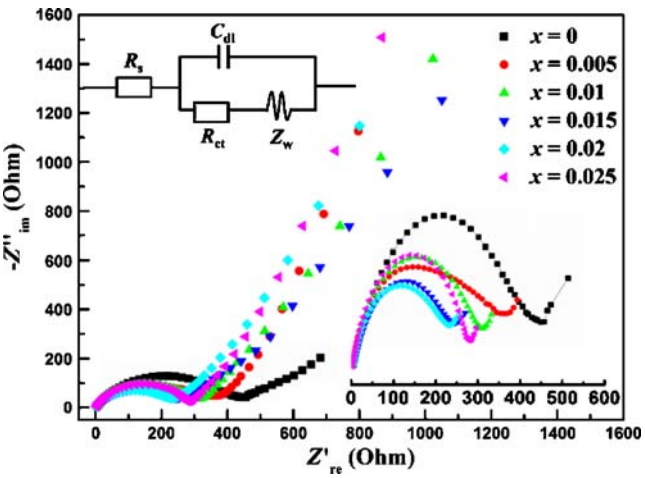

Fig. 9 EIS spectra of the $Li_{1-3x}La_xFePO_4/C$ (x=0, 0.005, 0.01, 0.015, 0.02, 0.025) samples. The *upper left inset* shows the equivalent circuit of the electrode. The *lower right inset* shows an enlargement of the high-frequency region

frequency region is attributed to the Warburg impedance (Z_w), which is associated with lithium ion diffusion [5]. Interpretation of the impedance spectra is based on a simplified equivalent circuit (as shown in the upper left inset of Fig. 9). The symbols C_{dl} and R_s denote the capacitance of the double layer and the solution resistance, respectively. It can be seen that the semicircle intercepts shift to the negative direction on the real axis with increasing doping level. The $Li_{1-3x}La_xFePO_4/C$ (x=0.02) material has the smallest resistance, which is in agreement with the CV and cycling profiles. This could be attributed to the better electrical contact due to the carbon shells on the $Li_{1-3x}La_xFePO_4$ cores and the improved intrinsic electrical conductivity after lanthanum doping.

Conclusions

Nanosized carbon-coated $Li_{1-3x}La_xFePO_4$ (x=0.005, 0.01, 0.015, 0.02, 0.025) materials with a core-shell structure were prepared by microwave-assisted, room-temperature, solid-state reaction. Citric acid was used in the process of synthesis to form a uniform and continuous carbon shell, which plays an important role in inhibiting the growth of particles and providing an electronic conductor. Testing results on the electronic conductivity indicate that the lanthanum substitution enhances the electronic conductivity, thus increasing the discharge capacity of the electrode materials. Impressively, the strategy of a combination of carbon coating and lanthanum doping is very promising for improving the electrochemical performance of $LiFePO_4$. Furthermore, the nanosized $Li_{1-3x}La_xFePO_4/C$ (x=0.02) cathode material consisting of small and uniform particles (25–50 nm) provides a high discharge capacity of 145 mA h/g at the discharge rate of 1.5 C, enhanced cycling stability, and good rate capability, which make it attractive for large-scale applications.

Acknowledgements This work was supported by grants from the Natural Science Foundation of Xinjiang Province (Nos. 200821121 and 200721102) and the National Natural Science Foundation of China (Nos. 20666005 and 20661003).

References

1. Padhi AK, Nanjundaswamy KS, Goodenough JB (1997) J Electrochem Soc 144:1188
2. Song M-S, Kang Y-M, Kim J-H, Kim H-S, Kim D-Y, Kwon H-S, Lee J-Y (2007) J Power Sources 166:260
3. Giorgetti M, Berrettoni M, Scaccia S, Passerini S (2006) Inorg Chem 45:2750
4. Wang Y, Wang Y, Hosono E, Wang K, Zhou H (2008) Angew Chem Int Ed 47:7461
5. Shin HC, Cho WI, Jang H (2006) Electrochim Acta 52:1472
6. Chung S-Y, Bloking JT, Chiang Y-M (2002) Nat Mater 1:123
7. Wang Y, Wang J, Yang J, Nuli Y (2006) Adv Funct Mater 16:2135
8. Liu H, Cao Q, Fu LJ, Li C, Wu YP, Wu HQ (2006) Electrochem Commun 8:1553
9. Jayaprakash N, Kalaiselvi N (2007) Electrochem Commun 9:620
10. Herle PS, Ellis B, Coombs N, Nazar LF (2004) Nat Mater 3:147
11. Wang GX, Bewlay SL, Konstantinov K, Liu HK, Dou SX, Ahn JH (2004) Electrochim Acta 50:443
12. Wang D, Li H, Shi S, Huang X, Chen L (2005) Electrochim Acta 50:2955
13. Liao X-Z, He Y-S, Ma Z-F, Zhang X-M, Wang L (2007) J Power Sources 174:720
14. Li X, Kang F, Bai X, Shen W (2007) Electrochem Commun 9:663
15. Dominko R, Bele M, Gaberscek M, Remskar M, Hanzel D, Goupil JM, Pejovnik S, Jamnik J (2006) J Power Sources 153:274
16. Sanchez MAE, Brito GES, Fantini MCA, Goya GF, Matos JR (2006) Solid State Ionics 177:497
17. Gaberscek M, Dominko R, Bele M, Remskar M, Hanzel D, Jamnik J (2005) Solid State Ionics 176:1801
18. Yang S, Song Y, Zavalij PY, Stanley Whittingham M (2002) Electrochem Commun 4:239
19. Yamada A, Chung SC, Hinokuma K (2001) J Electrochem Soc 148:A224
20. Prosini PP, Zane D, Pasquali M (2001) Electrochim Acta 46:3517
21. Arnold G, Garche J, Hemmer R, Ströbele S, Vogler C, Wohlfahrt-Mehrens M (2003) J Power Sources 119–121:247
22. Ye XR, Jia DZ, Yu JQ, Xin XQ, Xue Z (1999) Adv Mater 11:941
23. Wang R-Y, Jia D-Z, Zhang L, Liu L, Guo Z-P, Li B-Q, Wang J-X (2006) Adv Funct Mater 16:687
24. Gerbec JA, Magana D, Washington A, Strouse GF (2005) J Am Chem Soc 127:15791
25. Wang L, Huang Y, Jiang R, Jia D (2007) J Electrochem Soc 154: A1015
26. Wang L, Huang Y, Jiang R, Jia D (2007) Electrochim Acta 52:6778
27. Zhuang D, Zhao X, Xie J, Tu J, Zhu T, Cao G (2006) Acta Phys-Chim Sin 22:840
28. Morgan D, Van der Ven A, Ceder G (2004) Electrochem Solid-State Lett 7:A30
29. Guo ZP, Liu H, Bewlay S, Liu HK, Dou SX (2005) Synth Met 153:113
30. Hu YS, Guo YG, Dominko R, Gaberscek M, Jamnik J (2007) Adv Mater 19:1963
31. Cho Y-D, Fey G, Kao H-M (2008) J Solid State Electrochem 12:815
32. Yang R, Song X, Zhao M, Wang F (2009) J Alloys Compd 468:365
33. Ying J, Lei M, Jiang C, Wan C, He X, Li J, Wang L, Ren J (2006) J Power Sources 158:543
34. Zhou Y-K, He B-L, Zhou W-J, Li H-L (2004) J Electrochem Soc 151:A1052